# Carbon Formation on Stainless Steel 304H in the Convection Section of an Ethane Cracking Plant

Farshid Ramezanipour,[1] Anand Singh,[1] Scott Paulson,[1] Hany Farag,[2] Viola I. Birss,[1] Venkataraman Thangadurai[1,*]
[1]Department of Chemistry, University of Calgary, 2500 University Dr. NW, Calgary, AB, Canada T2N 1N4
[2]NOVA Chemicals Research & Technology Centre (NRTC), 2928 16 Street NE, Calgary, AB, Canada T2E 7K7
*Corresponding author: vthangad@ucalgary.ca

## Abstract

The coking of stainless steel 304H alloy (SS304H) has been investigated in ethane-steam mixtures in presence/absence of a few ppm of $H_2S$ at 700 ºC. In this, first detailed study of the influence of $H_2S$ on carbon morphology on SS304H, we show that the addition of $H_2S$ greatly altered the carbon morphology, in the long-term experiments (90 h). For shorter exposure times (4 h), carbon formation decreased as $H_2S$ concentration was increased. This improved carbon tolerance of SS304H is likely due to adsorption of sulfur on its surface. Addition of $H_2S$ did not change ethane cracking temperature or product distribution.

**Keywords.** Stainless steel 304H, coking, $H_2S$ exposure, sulfur adsorption, carbon morphology, carbon nanofibers

## 1. Introduction

The exposure of Fe- or Ni-based alloys to high temperature processes involving high carbon activity ($a_c$) gases leads to the deterioration of metal surfaces causing carburization, and in extreme cases the formation of small metal particles mixed with carbon, commonly known as metal dusting. In the case of Fe, metal dusting begins with the formation of iron carbides (e.g., $Fe_3C$, $Fe_5C_2$) on the metal surface when the carbon activity is greater than 1.[1-4] Further carbon deposition in the form of a graphite layer on the carbide surface results in a decrease in the carbon activity (to ca. 1) at the carbide/graphite interface. This causes the decomposition of $Fe_xC_y$ into C and Fe. The Fe atoms then diffuse through the graphite layer to the exposed surface, where they form Fe particles that facilitate further carbon formation. In the case of Ni, the intermediate carbide phase does not form and metal disintegration occurs due to the penetration of carbon into Ni.[4] It has been suggested that the Ni atoms diffuse through the graphite to reach the outer surface, where they agglomerate and form particles that further facilitate carbon formation.

The formation of carbon fibers has been observed on these metal surfaces under carburizing conditions, equivalent to a high carbon activity. For Fe alloys, the suggested mechanism[5] involves the formation of $Fe_3C$ on the surface, causing defects to form, due to the volume difference between the carbide and metallic Fe. The accumulation of carbon at the defects results in the development of cracks in the carbide layer. This is followed by gas diffusion through the cracks and continuous carbon deposition beneath the $Fe_3C$ particles, forming more $Fe_3C$ and causing further metal dusting. Also, carbon diffuses through the $Fe_3C$ particles and precipitates at defects, with the continuous precipitation of carbon beneath the $Fe_3C$ particles resulting in the formation of fibers, having carbide particles on their tips. In the case of

Ni alloys, where there is no carbide formation, the carbon first deposits on the surface and then diffuses through Ni, precipitating at defects. Continuous carbon accumulation at the defects then leads to the separation of the Ni particles from the bulk metal and generation of cracks on the surface. Carburizing gases, such as hydrocarbons, can diffuse through these cracks, resulting in the further deposition of carbon beneath the Ni particles, causing further metal dusting. The continuous precipitation of carbon beneath the Ni particles results in the formation of carbon fibers with Ni on their tips.[5]

Various methods have been suggested to inhibit coking and the subsequent carburization and metal dusting at carbon-exposed Ni and Fe-based surfaces. One of these involves the deposition of a protective oxide layer, such as Al oxide, Si oxide and/or Cr(III) oxide, selected due to the low solubility of carbon in oxides.[6-10] In some cases, the layers have been deposited on the metal surface using sputtering methods.[11] Also, alloys rich in Cr, Al or Si are more carbon tolerant as these components can form protective oxides at the surface of the alloy.[6] It has also been shown that the addition of sulfur species to the reactive gases can help minimize coking. It has been suggested that sulfur adsorbs on the metal surface, inhibiting the nucleation of graphite on the metal surface and thereby preventing metal dusting.[12,13]

Stainless steel 304H (SS304H), which contains 70% Fe, 18% Cr and 8% Ni, is one of the common alloys used for gas transport in the petrochemical industry. Therefore, coke formation and metal dusting of this alloy in both dry and humid $CO/H_2$ mixtures has been examined previously.[14-16] However, considering the wide-spread application of the SS304H alloy in the ethane cracking industry,[17] further work is still needed to better understand the coking behavior of this alloy in ethane-steam mixtures. In the present work, the effect of the addition of $H_2S$ to ethane-steam mixtures on the coking of SS304H has been studied under conditions similar to

those encountered in the convection section of the ethane cracker, used in the petrochemical industry. We show that while subjecting the SS304H coupons to the convection section conditions of an ethane furnace, the addition of $H_2S$ can reduce the amount of coke formation. We also show in this first detailed study of the influence of $H_2S$ on carbon morphology that the addition of 15 ppm $H_2S$ to the ethane-steam mixture caused significant changes to the carbon morphology on the SS304H substrate.

## 2. Experimental Methods

Commercial SS304H coupons, with dimensions of 20 mm × 10 mm × 1.7 mm and 10 mm × 4 mm × 1.7 mm, were used in this work. An experimental unit was designed to mix the appropriate gases and flow them over the SS304H coupons, placed in a quartz tube at 700 ºC in a horizontal tube furnace. The gases were humidified (30-70 wt%) and the gas lines were heated from the humidifier to the furnace to prevent steam condensation.

The experiments involving $H_2S$ were performed using He + 26 ppm $H_2S$ or ethane + 50 ppm $H_2S$ mixtures. These gases were diluted appropriately to obtain the desired ppm level of $H_2S$ for each experiment. The $H_2S$-containing gases bypassed the humidifier in all experiments. The steam to ethane weight ratio was adjusted to be similar to that reported in the ethane cracking industry, which is typically 0.3 to 0.4.[18,19]

Forty experiments with gas exposure times ranging from 1 h to 90 h were performed in this study. In all cases, after the ethane-steam treatment, the reactor was cooled under dry He before taking the SS304H coupon out for further analysis. The gas outlet from the furnace was connected to a Dycor ProLine Process Mass Spectrometer to analyze the outlet gas composition.

After each experiment, the reaction quartz tube was cleaned by heating to 900 ºC, while a flow of air (25 mL /min) was maintained to ensure that any deposited carbon was oxidized and removed.

The oxidation of the SS304H coupons, carried out in order to generate a protective oxide film on the surface, was performed by heating the coupons in an air-steam mixture between 600 $^{o}$C and 900 $^{o}$C, and is similar to condition being used in the industry. Steam acts as diluent and helps to controls the temperature during the air-steam decoking procedure in the industrial furnaces.[20] In all cases, Alicat Scientific mass flow-meters were used to control the gas flows.

X-ray diffraction experiments were performed on a Bruker D8 Advance powder X-ray diffractometer with Cu Kα radiation (40 kV and 40 mA). Energy-dispersive X-ray spectroscopy (EDS) and scanning electron microscopy (SEM) experiments were done using a Philips FEI XL30 instrument without sputtering. Cross-sectional SEM studies were done using a Zeiss Σigma VP field emission scanning electron microscope equipped with an Oxford INCA X-Act EDXS unit. The samples for the cross-sectional SEM were prepared by polishing the samples to a 0.3 μm finish and etching for 60 seconds using glyceregia (15 ml HCl +10 ml glycerol + 5 ml $HNO_3$). X-ray photoelectron spectroscopy (XPS) experiments were performed using a PHI VersaProbe 5000-XPS.

## 3. Results and Discussion

### *3.1. Formation of Oxide Layer and Initial Ethane Exposure*

The SS304H coupons were first exposed to an air-steam mixture to form an oxide layer on the surface. EDS analysis showed that pre-oxidation leads to Cr enrichment on the surface and a decrease in the Fe and Ni surface content, with the Cr:Fe ratio increasing from 0.3 to 0.5 and the Cr:Ni ratio increasing from 2.2 to 5.1. EDS analysis also showed that, after pre-oxidation, the

O:Cr ratio increased from 0.2 to 0.7. This is consistent with the formation of $Cr_2O_3$ on the surface, as also reported by others.[10]

XRD experiments were also performed on both the as-received and oxidized SS304H coupons (Fig. 1). The pattern for the as-received SS304H coupon (Fig. 1) is consistent with Fe with a face-centered-cubic ($a$ = 3.601(1) Å; space group $Fm$-3$m$) structure. The XRD pattern for the oxidized sample matches with those of Fe and $Cr_2O_3$ (Joint Committee on Powder Diffraction Standards (JCPDS) card number 74–0326, space group $R$-3$c$, and $a$ = 4.936(2) Å and $b$ = 13.726(4) Å).

Before studying the coking of the SS304H coupons in ethane-steam mixtures, initial tests were performed by treating the oxidized samples in dry ethane for 2 h, which resulted in the formation of a layer of carbon on the entire surface, as shown in Fig. 2a. SEM images of the pre-oxidized SS304H surface, before and after ethane exposure, are shown in Figs. 2b and 2c, respectively. Close examination of the carbon clusters indicate that they consist of many tightly bundled carbon fibers (Fig. 2d). The regions between these clusters appear to be covered with a layer of carbon fibers, which is less tightly packed than the fibers in the carbon clusters (Fig. 2e).

*3.2. Coking in Ethane-Steam Mixture and the Effect of $H_2S$*

Figures 3a-g show optical images of samples after exposure to ethane-steam mixtures containing a range of ppm amounts of $H_2S$ for 4 h at 700 $^oC$. The long (90 h) experiments, with and without the addition of $H_2S$, both resulted in carbon deposition on the metal surface (Figs. 3h and 3i), as well as on the inner wall of the quartz tube in which the sample exposure to ethane-steam-$H_2S$ took place. The deposition of pyrolytic carbon on the quartz tube suggests that it would also be deposited on the metal surface, in addition to the coking activated by the metal

surface, which should result in carbon fiber formation also called filamentous or catalytic coke. The carbon distribution on the metal surface is uniform for samples that were not exposed to $H_2S$ (Fig. 3h), but relatively non-uniform for those exposed to 15 ppm $H_2S$ (Fig. 3i) in the long (90 h) experiments.

SEM studies show for the first time, to the best of our knowledge, that the presence of $H_2S$ during ethane exposure results in a significant change in the morphology of the carbon on the SS304H alloy surface. As shown in Fig. 4a for the 90 h experiments, when no $H_2S$ was present in the gas mixture, a uniform layer of carbon fibers (~50 nm in diameter) is present on the SS304H surface. The carbon adhered well to the metal surface for samples that were not exposed to $H_2S$ and could not easily be removed by manual shaking. The presence of a layer of well - defined carbon fibers (Fig. 4a) suggests that the carbon formed on the SS304H alloy in the absence of $H_2S$ is predominantly catalytic in nature. Consistent with the optical results in Fig. 3i, the addition of 15 ppm $H_2S$ to the ethane-steam mixture results in the formation of carbon clusters, which seem to be composed of small particles and very thin and short fibers that are tightly entangled (Fig. 4b). This could be due to sulfur adsorption on the surface, which may alter the fiber formation mechanism, hence preventing the formation of the same type of carbon fibers that are obtained in the absence of $H_2S$. Adsorption of sulfur on the surface is also known to reduce the catalytic carbon formation.[12] Also, the carbon formed in the presence of $H_2S$ could be physically removed very easily suggesting that this carbon might have been formed by gas phase radical reactions and settled on the metal surface.[21] The above observations suggest that in the presence of $H_2S$, large portions of the carbon formed on the metal surface is predominantly pyrolytic in nature, rather than metal-induced (i.e. catalytic carbon). To confirm the

reproducibility of these observations, the experiments with and without $H_2S$ were repeated several times; with the resulting images all being consistent with the above results.

Experiments were conducted to check the effect of He, and 95 vol % He / 5 vol % $H_2$ on the carbon clusters formed on pre-oxidized SS304H coupons treated in ethane-steam in the presence of 15 ppm $H_2S$ for 90 h. These experiments were conducted to check if the carbon particles or the thin fibers in the carbon clusters changed shape or got gasified when exposed to He or He/$H_2$ atmospheres at 700 $^oC$. Zhang et al have shown in similar experiments at 700 $^oC$ that a gas containing 33.3 vol % $H_2$ in He gasified and removed the catalytic carbon formed on Fe coupons.[22] The catalytic carbon had $Fe_3C$ particles and on exposure to a gas containing 33.3 vol % $H_2$ in He, the $Fe_3C$ particles were converted to α-Fe particles, which then catalyzed the carbon gasification.[22] In this study two pre-oxidized SS304H coupons were treated in ethane-steam in the presence of 15 ppm $H_2S$ for 90 h to form the carbon clusters. One of the samples was then exposed to He and the other to a He:$H_2$ mixture with a volumetric ratio of 95:5 for 10 h at 700 $^oC$. The SEM studies (Fig. 5) of both samples showed that He and the He:$H_2$ gas had no effect on the shape or quantity of the carbon clusters. The carbon clusters did not gasify in the 95 He:5 $H_2$, probably because of the absence of catalytic metal particles in the carbon clusters, indicating that the carbon clusters might be made predominantly of pyrolitic carbon. The long-term exposure of the SS304H coupons to ethane-steam resulted in the formation of a large amount of carbon, with carbon deposition observed even on the inner wall of the quartz reaction tube. Therefore, to avoid large amounts of pyrolitic carbon deposition and to more clearly observe the effect of $H_2S$ on the metal-induced carbon fibers, further experiments were performed for 4-6 h. As shown in Fig. 3, experiments with various amounts of added $H_2S$ were carried out and, in all cases, a parallel experiment without $H_2S$ was performed for comparison.

All of the no-$H_2S$ experiments showed the formation of carbon on the metal surface (Fig. 3a). The experiments with $H_2S$ present resulted in a systematic decrease in carbon formation as the amount of $H_2S$ increased from 1 ppm to 2, 5, 7, and 10ppm (Figs. 3b-f). At > 10 ppm $H_2S$, no carbon was observed on the SS304H surface. It should be noted that the accuracy of the mass flow meters used for mixing gases is ~1%, leading to an error of ± 0.5 ppm in the $H_2S$ concentration. SEM studies show that the surface of the SS304H coupon exposed to ethane-steam in the presence of 25 ppm $H_2S$ for 6 h (Fig. 6a) appears to be carbon-free and is very similar to that of the pre-oxidized SS304H before ethane-steam exposure (Fig. 6b). Cross-sectional SEM studies done on the SS304H coupon exposed to ethane-steam in the presence of 25 ppm $H_2S$ for 6 h (Fig. 6c) also show that there is no surface damage after the ethane treatment.

It was also of interest to determine if the metal surface beneath the carbon layer on the SS304H coupons from the no-$H_2S$ experiments was similar in nature to that of a pre-oxidized sample. To determine if this is the case, the carbon layer formed on a SS304H coupon (Fig. 6d) was oxidized by heating to 900 ºC in flowing air for 5 minutes. As seen in Fig. 6e, the metal surface after the oxidation of the carbon is very similar to the surface of a pre-oxidized SS304H (Fig. 6b) before exposure to ethane/steam. EDS studies also show that the Fe:Cr and Fe:Ni ratios of 2.0 and 9.8, respectively, for the de-coked surfaces are very similar to the ratios for the pre-oxidized SS304H before exposure to ethane/steam, which are 2.1 and 10.1, respectively.

*3.3. X-ray photoelectron spectroscopy (XPS)*

XPS experiments were performed to better understand the role of $H_2S$ in minimizing coking and to detect the possible adsorption of sulfur on the SS304H surface. Figure 7 shows the

sulfur peak (169.29 eV) in the XPS spectrum of the surface of a SS304H coupon, exposed to ethane-steam + 1 ppm $H_2S$. The binding energy of this peak is consistent with sulfur in a sulfate group. The XPS analysis of a SS304H coupon treated in dry ethane + 50 ppm $H_2S$ also showed similar results, with a sulfur peak at 169.18 eV. It is known that $FeSO_4$ can form as a result of the oxidation of $FeS_2$, which might be what occurred during transfer of the sample to the XPS chamber.[23] Also, in work with related metals, such as Ni, it has been shown by XPS that the sulfur at the surface of bulk Ni sulfides is easily oxidized to sulfate after exposure to air.[24]

Relative to the background, the sulfur signal is very small, and thus it appears that only roughly one monolayer of sulfur is present, consistent with sulfur adsorption rather than bulk Fe sulfide formation. The adsorption of sulfur then minimizes coke formation on the surface, potentially forming a monolayer of $FeS_2$, consuming Fe atoms that would otherwise form carbides.

*3.4. Mass Spectrometry*

Mass spectrometry analysis of the gases exiting the quartz tube reactor was done to determine the onset temperature of ethane decomposition. In the mass spectrometer, ethane is ionized to a parent molecular ion with a relative molecular mass (m) to charge (z) ratio (m/z) of 30. Also, the parent molecular ion is further fragmented to smaller ions with m/z ratios of 28, 27, 26 and 29 in the order of decreasing intensities. The fragmentation pattern of ethane shows that the fragmented ion with m/z ratio of 28 has a higher intensity than the parent ion with m/z ratio of 30.

In this study, the change in intensity of ions with m/z ratios of 30, 28, 26, 2, 18 and 16 were noted as a function of the temperature of the gas in the quartz tube reactor (Fig. 8). Helium gas

with m/z ratio of 4 was used as the internal standard and the signal strengths of the different ions were standardized with respect to the He signal. Ethane decomposition commences at ~600 ºC, as shown by the sudden decrease in the 30 m/z (ethane) signal intensity (Fig. 8). Also, there is a very sharp increase in the 2 m/z (hydrogen) signal intensity and a somewhat less pronounced increase in the 26 m/z ($C_2H_2$), and 16 m/z ($CH_4$) species signals (Fig. 8).

To determine the potential catalytic effect of the SS304H coupon itself on the cracking products obtained, another experiment was performed without a SS304H coupon present by flowing the ethane-steam mixture through the empty quartz tube, followed by mass spectrometry analysis of the exhaust gases. The results were very similar to those shown in Fig. 8, indicating that the metal coupon does not have any significant catalytic effect on the ethane cracking mechanism. To determine the effect of $H_2S$ on the ethane cracking temperature and product distribution, experiments were repeated by passing ethane-steam-$H_2S$ mixtures over the SS304H coupons from room temperature to 700 $^oC$. $H_2S$ did not have any significant influence on the ethane cracking initiation temperature or the product distribution.

**Conclusions**

The role of $H_2S$ in the minimization of carbon formation on SS304H alloys, used in the ethane cracking industry, has been studied here by exposure to ethane-steam mixtures under convection section conditions. It has been shown that a few ppm of $H_2S$ can greatly alter the morphology of the carbon, converting it from individual fibers into clusters composed of small particles and very thin and short fibers. Decreasing the ethane-steam exposure time resulted in an improved capability of detecting the impact of $H_2S$ in preventing coking. For example, in a series

of 4 hour experiments, a systematic decrease in carbon formation could be visually observed as the $H_2S$ concentration was increased.

The addition of 10 ppm $H_2S$ under our experimental conditions, which are comparable to those of the convection section, completely prevents carbon formation on the SS304H surface in the 4 hour experiments. XPS analysis confirms the presence of roughly one monolayer of sulfur on the $H_2S$-exposed surface, even with exposure to only 1 ppm $H_2S$. Finally, while the addition of $H_2S$ clearly minimizes catalytic carbon formation, it does not have an effect on the ethane cracking initiation temperature or on the ethane cracking mechanism in the convection section, as seen from the similarity in the products obtained with and without a SS304H sample present.

**Acknowledgements**

Authors thank the Natural Sciences and Engineering Research Council of Canada (NSERC) for supporting this work under the Strategic Project Grants (SPG) program. The authors would also like to thank Parastoo Keyvanfar, University of Calgary, for preparing the metallographic cross-sections for the SEM analysis.

**References**

[1] Q. Wei, E. Pippel, J. Woltersdorf and H.J. Grabke: 'Microprocesses of coke formation in metal dusting', *Mater. Corros.*, 1999, **50,** 628-633.

[2] J. Zhang, A. Schneider and G. Inden: 'Characterisation of the coke formed during metal dusting of iron in CO-$H_2$-$H_2O$ gas mixtures', *Corros. Sci.*, 2003, **45**, 1329-1341.

[3] C. M. Chun, J. D. Mumford and T. A. Ramanarayanan: 'Mechanisms of metal dusting corrosion of iron', *J. Electrochem. Soc.* 2002**, 149**, B348-B355.

[4] E. Pippel, J. Woltersdorf and R. Schneider: 'Micromechanisms of metal dusting on Fe-base and Ni-base alloys', *Mater. Corros.*, 1998, **49**, 309-316.

[5] Z. Zeng and K. Natesan: 'Relationship between the growth of carbon nanofilaments and metal dusting corrosion, *Chem. Mater.*, 2005, **17***,* 3794-3801.

[6] H.J. Grabke and I. Wolf: 'Carburization and oxidation', *Mater. Sci. Eng.*, 1987, **87**, 23-33.

[7] H.J. Grabke: 'Nickel-based alloys in carbonaceous gases', *Corrosion*, 2000, **56**, 801-808.

[8] H. Liu and W. Chen: 'Effect of pre-oxidation on coke formation and metal dusting of electroplated $Ni_3Al$–$CeO_2$-based coatings in CO–$H_2$–$H_2O$', *Mater. Corros.* 2008, **59**, 311-318.

[9] H.J. Grabke, R. Krajak, E.M. Miiller-Lorenz and S. Strauß: 'Metal dusting of nickel-base alloys', *Mater. Corros*. 1996*,* **47**, 495-504.

[10] D. J. Young, J. Zhang, C. Geers and M. Schütze: 'Recent advances in understanding metal dusting: A review', *Mater. Corros,.* 2011, **62**, 7-28.

[11] L.M. López, O. Salas, L. Melo-Máximo, J. Oseguera, C.M. Lepienski, P. Soares, R.D. Torres and R.M. Souza: 'Structural and mechanical analysis for the optimization of PVD oxide coatings for protection against metal dusting', *Appl. Surf. Sci.*, 2012, **258**, 7306-7313.

[12] H. J. Grabke, D. Moszynski, E. M. Müller-Lorenz and A. Schneider: 'Role of sulphur in carburization, carbide formation and metal dusting of iron', *Surf. Interface Anal.*, 2002**, 34***,* 369-374.

[13] A. Schneider and H. J. Grabke: 'Effect of $H_2S$ on metal dusting of iron', *Mater. Corros.*, 2003, **54**, 793-798.

[14] J. Zhang, K. Boddington and D. J. Young: 'Oxidation, carburisation and metal dusting of 304 stainless steel in $CO/CO_2$ and $CO/H_2/H_2O$ gas mixtures:, *Corros. Sci.*, 2008, **50**, 3107-3115.

[15] P. Szakalos, R. Pettersson and S. Hertzman: 'An active corrosion mechanism for metal dusting on 304L stainless steel' *Corros. Sci.*, 2002, **44**, 2253-2270.

[16] C. M. Chun and T. A. Ramanarayanan: 'Metal Dusting Corrosion of Austenitic 304 Stainless Steel', *J. Electrochem. Soc.*, 2005, **152**, B169-B177.

[17] J. Xie, M. Crawford, L. Davies, D. Eisenhawer, R. Saunders and L. Benum: 'An approach to determine the initiation of carburization in a 304H stainless steel piping under petrochemical environment'**,** *Corrosion Conference and Expo - NACE International*, 2011, **4**, 3080-3089.

[18] A. M. Gujarathi, D. S. Patle, P. Agarwal, A. L. Karemore and B. V. Babu: 'Simulation and Analysis of Ethane Cracking Process', in 'Proceedings of International Symposium & 62nd Annual Session of IIChE (CHEMCON-2009)', 2009, Visakhapatnam, India.

[19] Q. Chen, E. J. A. Schweitzer, P. F. Van Den Oosterkamp, R. J. Berger, C. R. H. De Smet and G. B. Marin: 'Oxidative pyrolysis of ethane', *Ind. Eng. Chem. Res.*, 1997, **36***,* 3248-3251.

[20] R. A. Hill, INEOS Olefins & Polymers USA,: 'Medium pressure steam intervention in an olefin cracking furnace decoke procedure', US Patent 0060586, 6 March 2014.

[21] H. Cai, A. Krzywicki and M. C. Oballa: 'Coke formation in steam crackers for ethylene production' Chem. Eng. Process. 2002, **41**, 199–214.

[22] J. Zhang, A. Schneider and G. Inden: 'Cementite decomposition and coke gasification in He and $H_2$–He gas mixtures', *Corros. Sci.*, 2004, **46**, 667-679.

[23] E. C. Todd, D. M. Sherman and J. A. Purton: 'Surface oxidation of pyrite under ambient atmospheric and aqueous (pH =2 to 10) conditions: Electronic structure and mineralogy from X-ray absorption spectroscopy', *Geochim. Cosmochim. Acta,* 2003*,* **67***,* 881-893.

[24] D. L. Legrand, H. W. Nesbitt and G. M. Bancroft: 'X-ray photoelectron spectroscopic study of a pristine millerite (NiS) surface and the effect of air and water oxidation', *Am. Mineral.*, 1998*,* **83***,* 1256-1265.

## Figure Captions

**Figure 1.** Powder X-ray diffraction analysis of (a) an as-received stainless steel 304H coupon, showing a face-centered-cubic iron (*Fm*-3*m*) structure and (b) after pre-oxidation of SS304H in an air-steam mixture, showing primarily $Cr_2O_3$ (*JCPDS card no* 74–0326) on FCC Fe.

**Figure 2. (a)** Optical images of pre-oxidized SS304 H coupons before and after exposure to dry ethane. SEM images of (b) the pre-oxidized surface, **(c)** an ethane-exposed surface (700 ºC for 6 h), **(d)** a close look at one of the carbon clusters observed in (c), and **(e)** the area between the carbon clusters.

**Figure 3.** Optical views of pre-oxidized SS304H coupons exposed for 4 h at 700 ºC to ethane-steam mixtures containing **(a)** no $H_2S$ **(b)** 1 ppm $H_2S$, **(c)** 2 ppm $H_2S$, **(d)** 5 ppm $H_2S$, **(e)** 7 ppm $H_2S$, and **(f)** 10 ppm $H_2S$. Optical views of pre-oxidized SS304H coupons **(g)** before exposure to ethane-steam, **(h)** after exposure to ethane-steam for 90 h in the absence of $H_2S$ **(i)** after exposure to ethane-steam for 90 h in the presence of 15 ppm $H_2S$.

**Figure 4.** SEM images of the pre-oxidized stainless steel 304H coupons exposed for 90 h to **(a)** ethane-steam and **(b)** ethane-steam containing 15 ppm $H_2S$. Note the fibers seen in the no-$H_2S$ case and the cluster-like carbon seen for the sample exposed to $H_2S$.

**Figure 5.** SEM images of the pre-oxidized stainless steel 304H samples exposed to **(a)** ethane-steam + 15 ppm $H_2S$, **(b)** ethane-steam + 15 ppm $H_2S$, followed by 10 hour exposure to He and

**(c)** ethane-steam + 15 ppm $H_2S$ followed by a 10 hour exposure to He:$H_2$ mixture in a volumetric ratio of 95:5.

**Figure 6.** SEM images of pre-oxidized SS304H coupons **(a)** after exposure to ethane-steam + 25 ppm $H_2S$ for 6 h, **(b)** before exposure to ethane-steam, **(c)** cross-section after exposure to ethane-steam + 25 ppm $H_2S$ for 6 h, showing no damage to the surface, **(d)** after exposure to ethane-steam for 4 h, showing carbon fibers on the surface, and **(e)** after exposure to ethane-steam (to form carbon fibers on the surface), followed by decoking in air at 900 $^oC$. Note that the surface of SS304H in **(a)**, **(b)** and **(e)** look similar, showing that exposure to ethane-steam + 25 ppm $H_2S$ or one coking decoking cycle does not affect the surface of the SS304H coupons**.**

**Figure 7.** XPS analysis of stainless steel 304H sample, exposed to ethane-steam + 1 ppm $H_2S$. The peak position at 169.29 eV indicates that sulfur is present primarily in the sulfate form.

**Figure 8.** Mass spectrometry data of the ethane-steam gas mixture exiting the quartz tube reactor containing a SS304H coupon showing the changes in intensities of the molecular mass of the various fragments due to ethane cracking. The quartz tube with the SS304H coupon was heated to 700 $^oC$ and the changes in intensities of the molecular mass of the various fragments are plotted as a function of time and temperature. The heating of the furnace started after 0.7 h and the temperature reached 700 °C after 2.4 h. After 2.4 hours, the furnace temperature was maintained at 700 °C. The signals for species with molecular masses 26 and 16 are enlarged on the right.

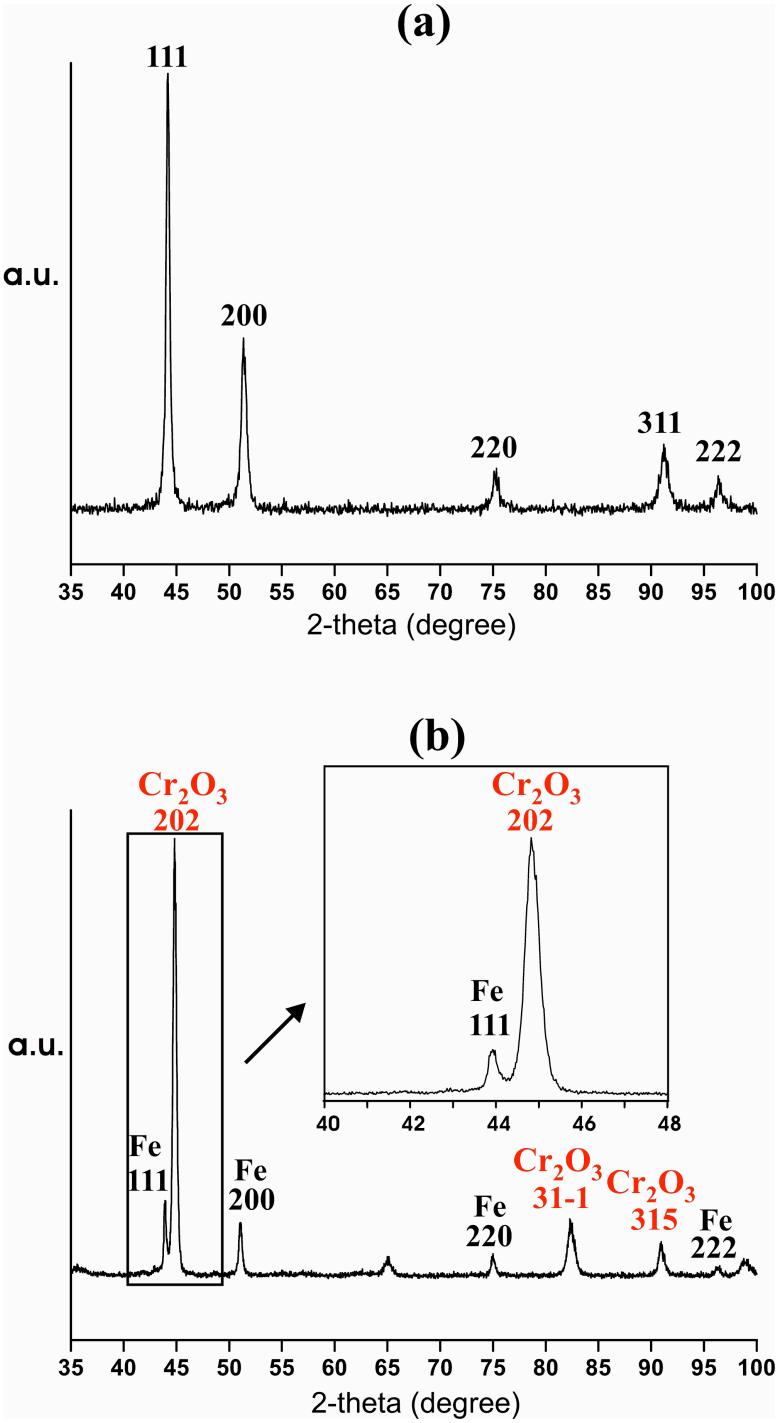


**Figure 1.** Powder X-ray diffraction analysis of (a) an as-received stainless steel 304H coupon, showing a face-centered-cubic iron (*Fm*-3*m*) structure and (b) after pre-oxidation of SS304H in an air-steam mixture, showing primarily $Cr_2O_3$ (*JCPDS card no* 74–0326) on FCC Fe.

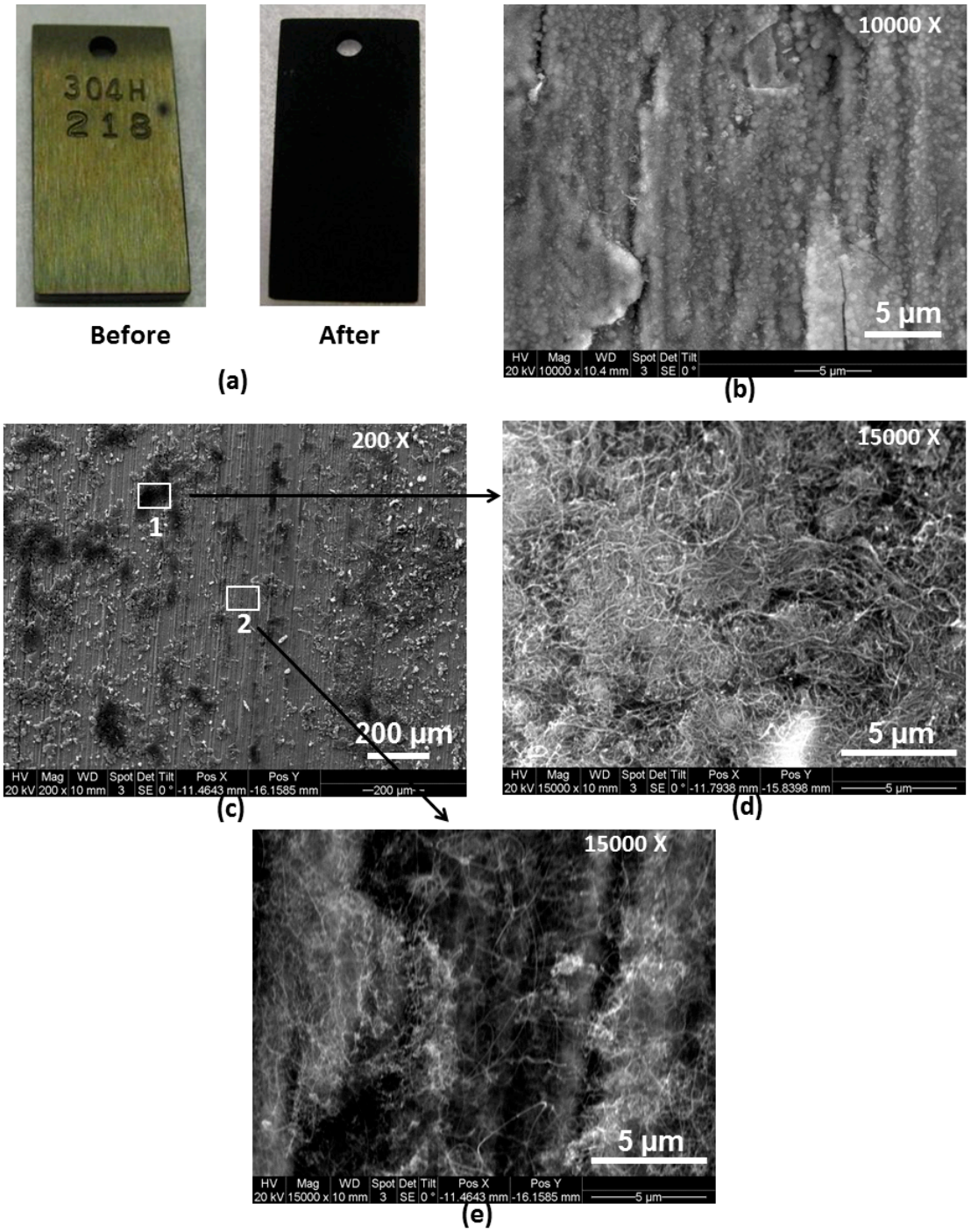


**Figure 2. (a)** Optical images of pre-oxidized SS304 H coupons before and after exposure to dry ethane. SEM images of (b) the pre-oxidized surface, **(c)** an ethane-exposed surface (700 ºC for 6 h), **(d)** a close look at one of the carbon clusters observed in (c), and **(e)** the area between the carbon clusters.

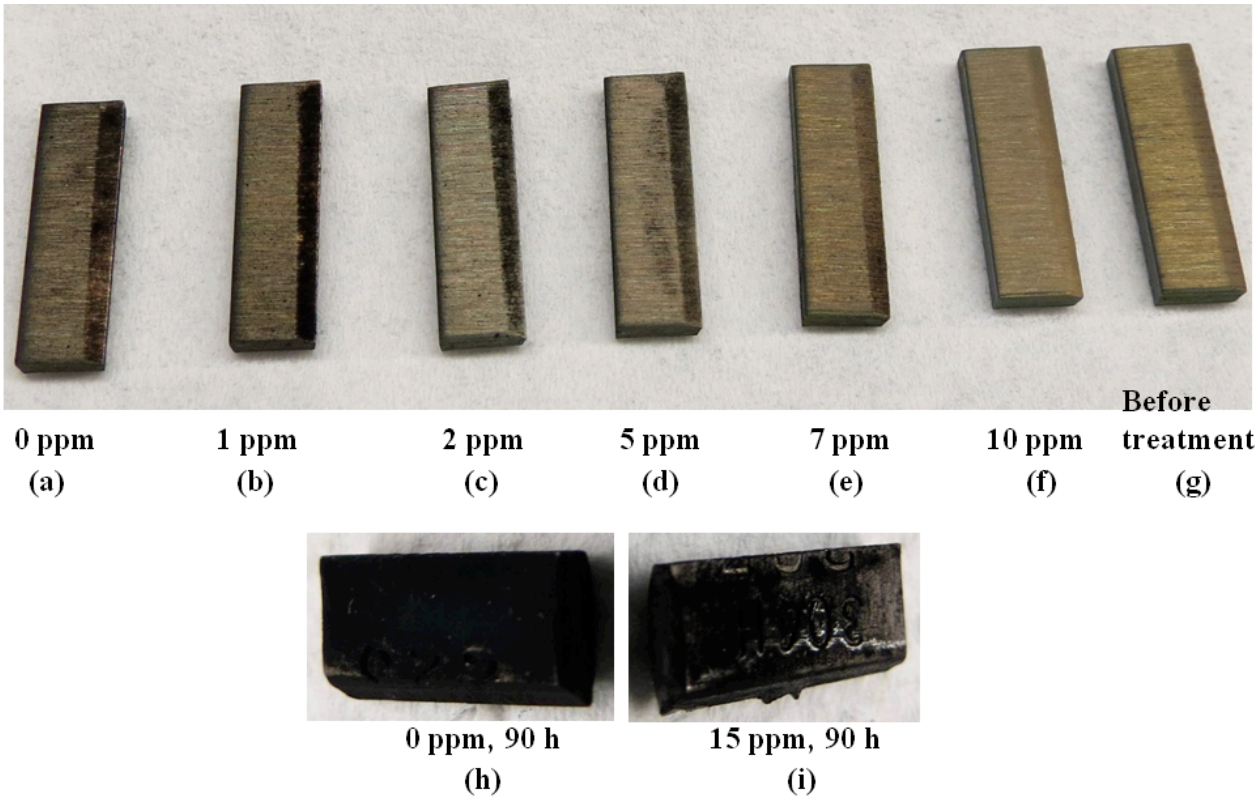


**Figure 3.** Optical views of pre-oxidized SS304H coupons exposed for 4 h at 700 ºC to ethane-steam mixtures containing **(a)** no $H_2S$ **(b)** 1 ppm $H_2S$, **(c)** 2 ppm $H_2S$, **(d)** 5 ppm $H_2S$, **(e)** 7 ppm $H_2S$, and **(f)** 10 ppm $H_2S$. Optical views of pre-oxidized SS304H coupons **(g)** before exposure to ethane-steam, **(h)** after exposure to ethane-steam for 90 h in the absence of $H_2S$ **(i)** after exposure to ethane-steam for 90 h in the presence of 15 ppm $H_2S$.

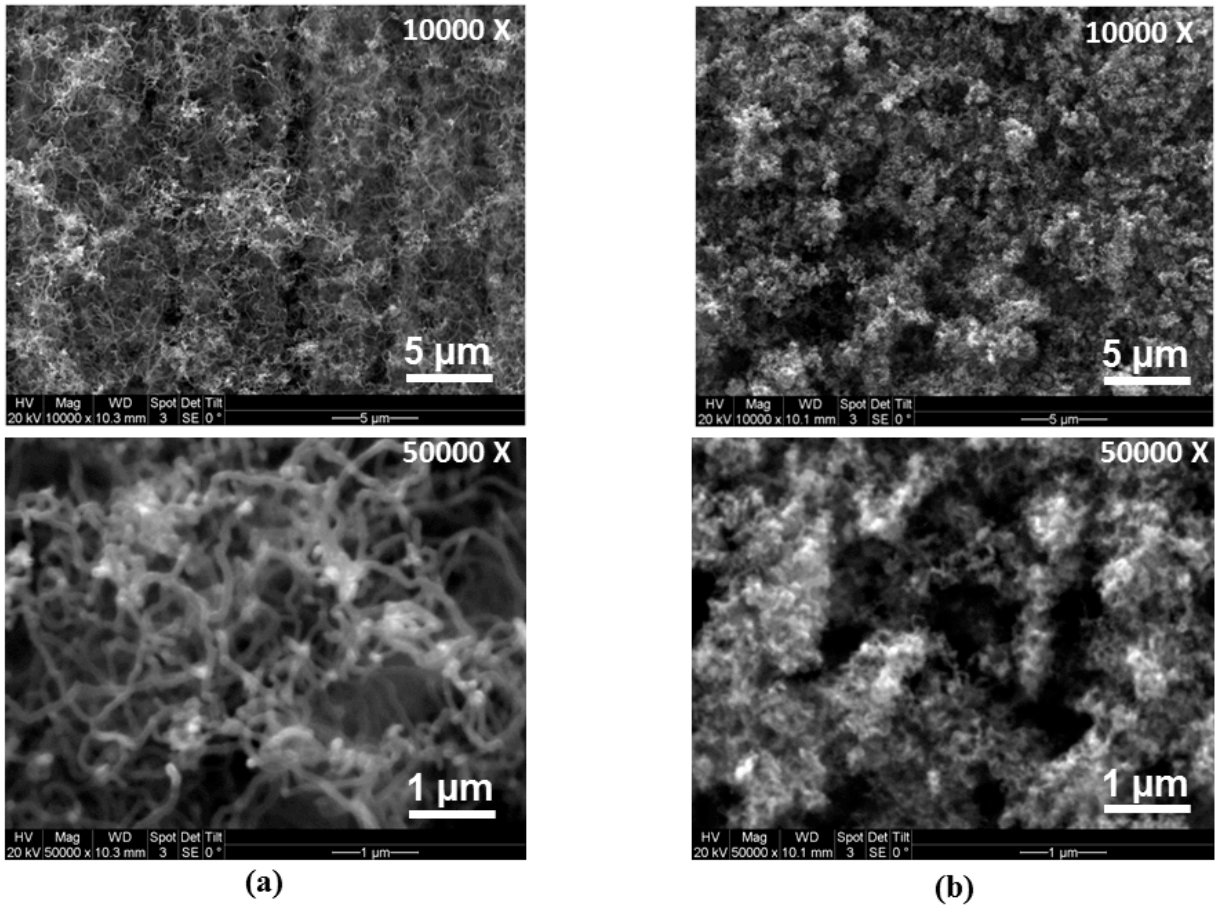


**Figure 4.** SEM images of the pre-oxidized stainless steel 304H coupons exposed for 90 h to **(a)** ethane-steam and **(b)** ethane-steam containing 15 ppm $H_2S$. Note the fibers seen in the no-$H_2S$ case and the cluster-like carbon seen for the sample exposed to $H_2S$.

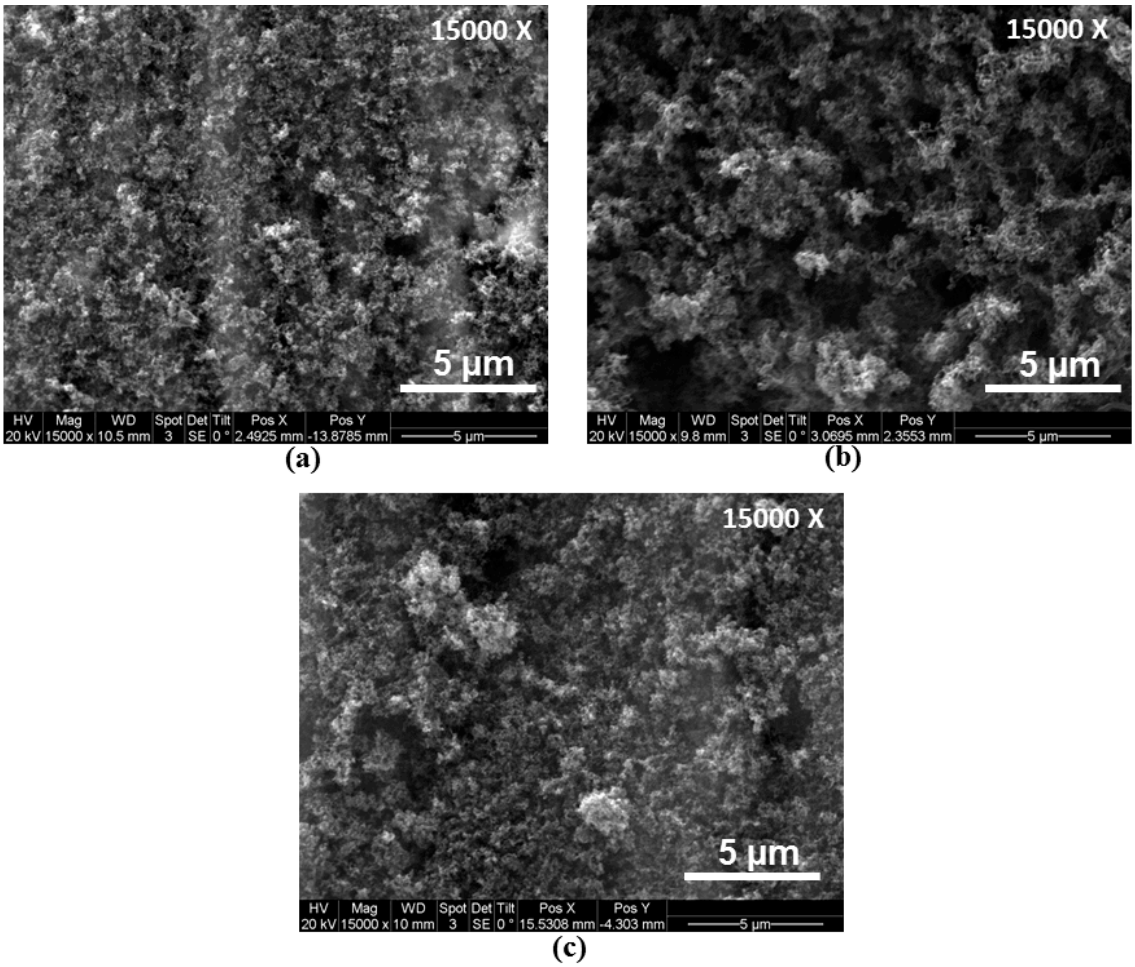


**Figure 5.** SEM images of the pre-oxidized stainless steel 304H samples exposed to **(a)** ethane-steam + 15 ppm $H_2S$, **(b)** ethane-steam + 15 ppm $H_2S$, followed by 10 hour exposure to He and **(c)** ethane-steam + 15 ppm $H_2S$ followed by a 10 hour exposure to He:$H_2$ mixture in a volumetric ratio of 95:5.

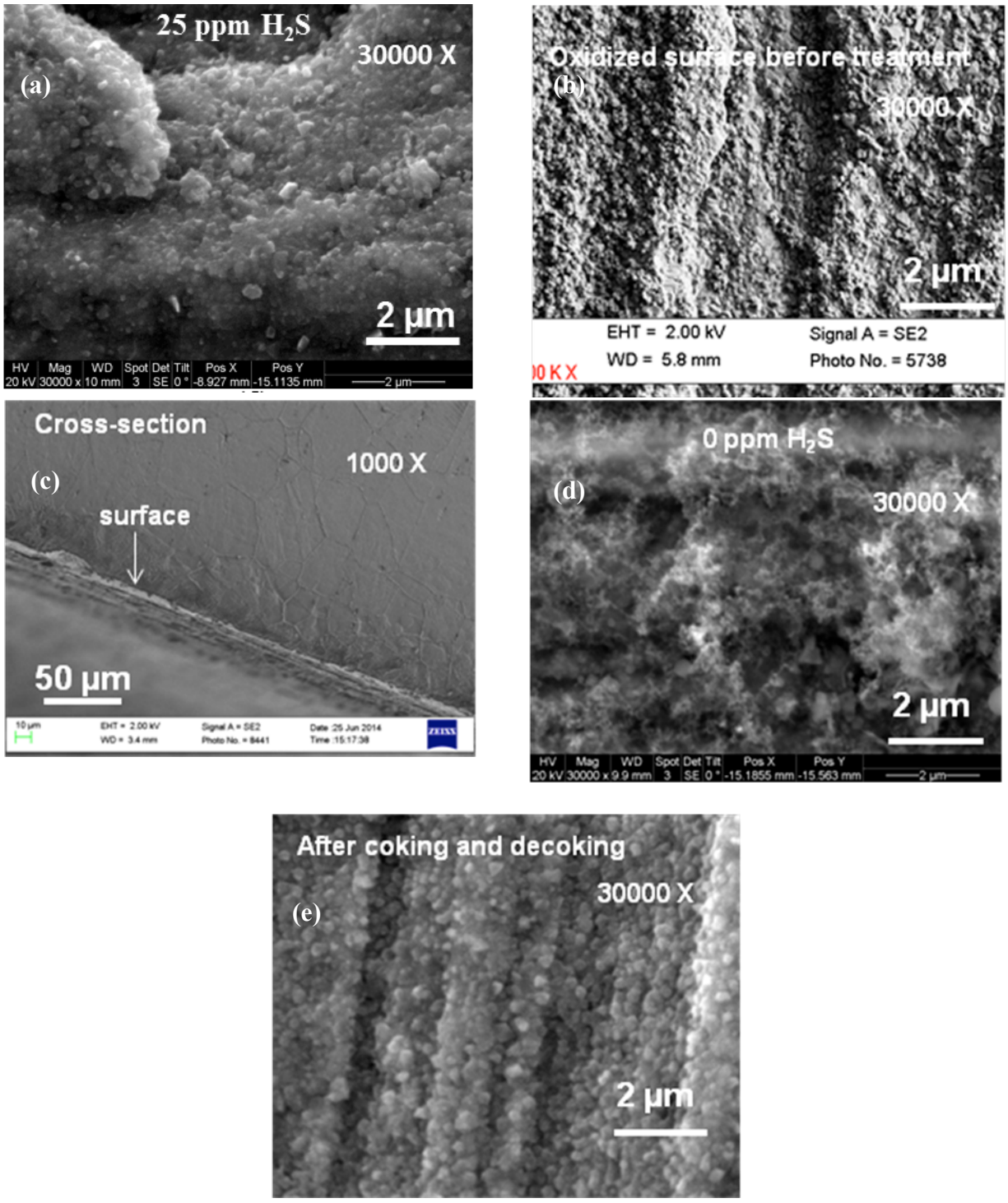


**Figure 6.** SEM images of pre-oxidized SS304H coupons **(a)** after exposure to ethane-steam + 25 ppm $H_2S$ for 6 h, **(b)** before exposure to ethane-steam, **(c)** cross-section after exposure to ethane-steam + 25 ppm $H_2S$ for 6 h, showing no damage to the surface, **(d)** after exposure to ethane-steam for 4 h, showing carbon fibers on the surface, and **(e)** after exposure to ethane-steam (to form carbon fibers on the surface), followed by decoking in air at 900 $^{o}$C. Note that the surface

of SS304H in **(a)**, **(b)** and **(e)** look similar, showing that exposure to ethane-steam + 25 ppm $H_2S$ or one coking decoking cycle does not affect the surface of the SS304H coupons**.**

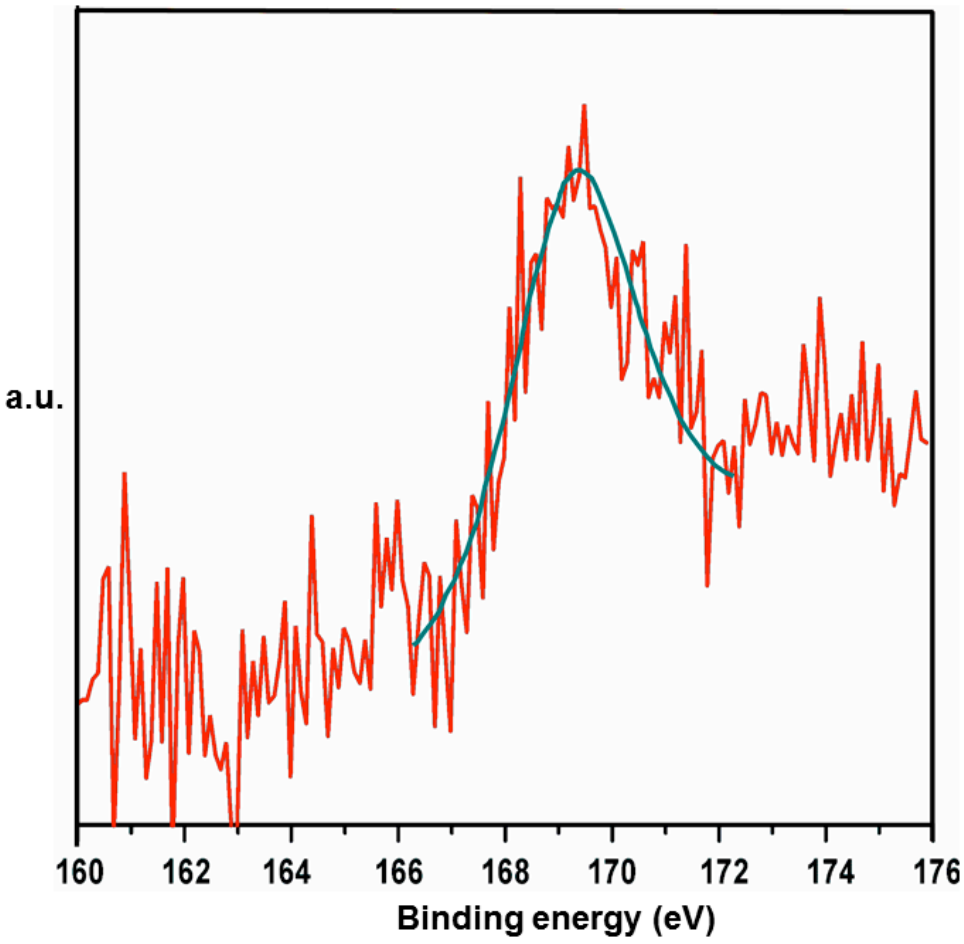


**Figure 7.** XPS analysis of stainless steel 304H sample, exposed to ethane-steam + 1 ppm $H_2S$. The peak position at 169.29 eV indicates that sulfur is present primarily in the sulfate form.

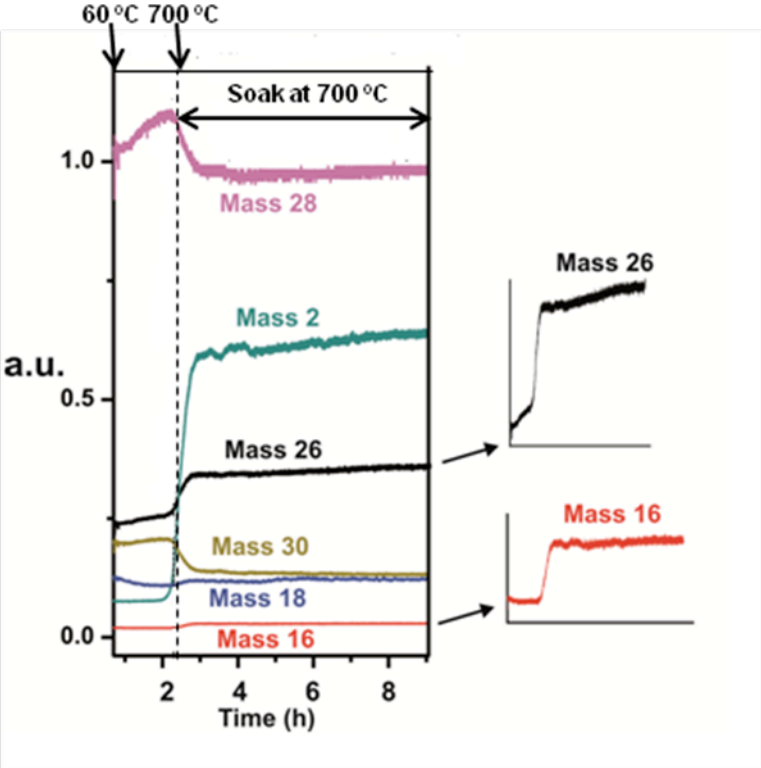


**Figure 8.** Mass spectrometry data of the ethane-steam gas mixture exiting the quartz tube reactor containing a SS304H coupon showing the changes in intensities of the molecular mass of the various fragments due to ethane cracking. The quartz tube with the SS304H coupon was heated to 700 $^{o}$C and the changes in intensities of the molecular mass of the various fragments are plotted as a function of time and temperature. The heating of the furnace started after 0.7 h and the temperature reached 700 °C after 2.4 h. After 2.4 hours, the furnace temperature was maintained at 700 °C. The signals for species with molecular masses 26 and 16 are enlarged on the right.